

RELATIONSHIP BETWEEN THE GAMMA-RAY BURST PULSE WIDTH AND ENERGY DUE TO THE DOPPLER EFFECT OF FIREBALLS

Y.-P. QIN,^{1,2} Y.-M. DONG,^{1,3} R.-J. LU,^{1,2,3} B.-B. ZHANG,^{1,3} AND L.-W. JIA^{1,3}

Received 2004 September 24; accepted 2005 June 29

ABSTRACT

We study in detail how the pulse width of gamma-ray bursts is related to energy under the assumption that the sources concerned are in the fireball stage. Due to the Doppler effect of fireballs, there exists a power-law relationship between the two quantities within a limited range of frequency. The power-law range and power-law index depend strongly on the observed peak energy E_p as well as the rest-frame radiation form, and the upper and lower limits of the power-law range can be determined by E_p . It is found that within the same power-law range, the ratio of the FWHM of the rising portion to that of the decaying phase of the pulses is also related to energy in the form of power laws. A plateau/power law/plateau feature is observed in the two relationships. In the case of an obvious softening of the rest-frame spectrum, the two power-law relationships also exist, but the feature evolves to a peaked one. Predictions of the relationships in the energy range covering both the BATSE and *Swift* bands for a typical hard burst and a typical soft one are made. A sample of FRED (fast rise and exponential decay) pulse bursts shows that 27 out of the 28 sources belong to either the plateau/power law/plateau feature class or to the peaked feature group, suggesting that the effect concerned is indeed important for most of the sources of the sample. Among these bursts, many might undergo an obvious softening evolution of the rest-frame spectrum.

Subject headings: gamma rays: bursts — gamma rays: theory — relativity

1. INTRODUCTION

Owing to the large amount of energy observed, gamma-ray bursts (GRBs) were assumed to undergo a relativistically expanding fireball stage (see, e.g., Goodman 1986; Paczyński 1986). Relativistic bulk motion of the gamma-ray-emitting plasma plays a role in producing the observed phenomena of the sources (Krolik & Pier 1991). It was believed that the Doppler effect over the whole fireball surface (the so-called relativistic curvature effect) might be the key factor to account for the observed spectrum of the events (see, e.g., Mészáros & Rees 1998; Hailey et al. 1999; Qin 2002, 2003).

Some simple bursts with well-separated structure suggest that they may consist of fundamental units of radiation such as pulses, with some of them being seen to comprise fast rise and an exponential decay (FRED) phases (see, e.g., Fishman et al. 1994). These FRED pulses could be well represented by flexible empirical or quasi-empirical functions (see, e.g., Norris et al. 1996; Kocevski et al. 2003). Fitting the corresponding light curves with the empirical functions, many statistical properties of pulses were revealed. Light curves of GRB pulses were found to become narrower at higher energies (Fishman et al. 1992; Link et al. 1993). Fenimore et al. (1995) showed that the average pulse width is related to energy by a power law with an index of about -0.4 . This was confirmed by later studies (Fenimore et al. 1995; Norris et al. 1996, 2000; Costa 1998; Piro et al. 1998; Nemiroff 2000; Feroci et al. 2001; Crew et al. 2003).

In the past few years, many attempts at interpretation of light curves of GRBs have been made (see, e.g., Fenimore et al. 1996; Norris et al. 1996, 2000; Ryde & Petrosian 2002; Kocevski et al. 2003). It has been suggested that the power-law relationship can be attributed to synchrotron radiation (see Fenimore et al. 1995;

Cohen et al. 1997; Piran 1999). Kazanas et al. (1998) proposed that the relationship can be accounted for by synchrotron cooling (see also Chiang 1998; Dermer 1998; Wang et al. 2000). Phenomena such as the hardness-intensity correlation and the FRED form of pulses were recently interpreted as signatures of the relativistic curvature effect (Fenimore et al. 1996; Ryde & Petrosian 2002; Kocevski et al. 2003; Qin et al. 2004, hereafter Paper I). It was suspected that the power-law relationship might result from a relative projected speed or a relative beaming angle (Nemiroff 2000). Due to the feature of self-similarity across the energy bands observed (see, e.g., Norris et al. 1996), it is likely that the observed difference between the light curves of the different channels might mainly be due to the energy channels themselves. In other words, light curves of different energy channels might arise from the same mechanism (e.g., parameters of the rest-frame spectrum and parameters of the expanding fireballs are the same for different energy ranges), differing only in the energy ranges involved.

We believe that if different-channel light curves of a burst can be accounted for by the same mechanism, where except for the energy ranges concerned no parameters are allowed to be different for the different energy channels, then the mechanism must be the main cause of the observed difference. A natural mechanism that possesses this property might be the Doppler effect of the expanding fireball surface when a rest-frame radiation form is assumed. Indeed, as shown in Paper I, the four-channel light curves of GRB 951019 were found to be well fitted by a single formula derived when this effect was taken into account. In Paper I the power-law relationship between the pulse width and energy was interpreted as being mainly due to different active areas of the fireball surface corresponding to the majority of photons of these channels. However, how the width is related to energy remains unclear. In the following we present a detailed analysis of this issue, and on the basis of our analysis we make predictions of this relationship over a wide range covering both the BATSE and *Swift* bands.

This paper is organized as follows. In § 2 we investigate in a general manner how the width and the ratio of the rising width to

¹ National Astronomical Observatories/Yunnan Observatory, Chinese Academy of Sciences, P.O. Box 110, Kunming, Yunnan 650011, China; ypqin@ynao.ac.cn.

² Physics Department, Guangxi University, Nanning, Guangxi 530004, China.

³ Graduate School of the Chinese Academy of Sciences, P.O. Box 3908, Beijing 100039, China.

the decaying width of GRB pulses are related to energy. Then we make predictions of the relationship over the BATSE and *Swift* bands for typical hard and soft bursts in § 3. In § 4 a sample containing 28 FRED pulse sources is employed to illustrate the relationship. A brief discussion and our conclusions are presented in the last section.

2. GENERAL ANALYSIS OF THE RELATIONSHIP

Studies of the Doppler effect of the expanding fireball surface were presented by different authors, and based on these studies formulae applicable to various situations are available (see, e.g., Fenimore et al. 1996; Granot et al. 1999; Eriksen & Gron 2000; Dado et al. 2002a, 2002b; Ryde & Petrosian 2002; Kocevski et al. 2003; Paper I; Shen et al. 2005). In the following we employ one of them that is suitable for studying the issue noted above, where a highly symmetric and expanding fireball is concerned.

It can be verified that the expected flux of a fireball expanding with a Lorentz factor $\Gamma > 1$ can be determined by (for a detailed derivation the formula one can refer to Paper I)

$$f_\nu(\tau) = \frac{2\pi R_c^2}{D^2 \Gamma^3 (1 - \beta)^2 \{1 + [\beta/(1 - \beta)]\tau\}^2} \times \int_{\tilde{\tau}_{\theta, \min}}^{\tilde{\tau}_{\theta, \max}} \tilde{I}(\tau_\theta) (1 + \beta\tau_\theta)^2 (1 - \tau + \tau_\theta) g_{0, \nu}(\nu_{0, \theta}) d\tau_\theta, \quad (1)$$

with $\tau_{\min} \leq \tau \leq \tau_{\max}$, $\tau_{\min} \equiv (1 - \beta)\tau_{\theta, \min}$, $\tau_{\max} \equiv 1 + \tau_{\theta, \max}$, $\tau \equiv (t - D/c + R_c/c - t_c)/(R_c/c)$, and $\tau_\theta \equiv (t_\theta - t_c)/(R_c/c)$, where t is the observation time measured by the distant observer, t_θ is the local time measured by the local observer located at the place encountering the expanding fireball surface at the position θ relative to the center of the fireball, t_c is the initial local time, R_c is the radius of the fireball measured at $t_\theta = t_c$, D is the distance from the fireball to the observer, $\tilde{I}(\tau_\theta)$ represents the development of the intensity measured by the local observer, and $g_{0, \nu}(\nu_{0, \theta})$ describes the rest-frame radiation; $\nu_{0, \theta} = (1 - \beta + \beta\tau)\Gamma\nu/(1 + \beta\tau_\theta)$, $\tilde{\tau}_{\theta, \min} = \max\{\tau - 1, \tau_{\theta, \min}\}$, and $\tilde{\tau}_{\theta, \max} = \min\{\tau/(1 - \beta), \tau_{\theta, \max}\}$, with $\tau_{\theta, \min} = (t_{\theta, \min} - t_c)/(R_c/c)$ and $\tau_{\theta, \max} = (t_{\theta, \max} - t_c)/(R_c/c)$ being the upper and lower limits of τ_θ confining $\tilde{I}(\tau_\theta)$, respectively. (Note that since the limit of the Lorentz factor is $\Gamma > 1$, the formula can be applied to the cases of relativistic, subrelativistic, and nonrelativistic motions.)

The expected count rate of the fireball measured within frequency interval $[\nu_1, \nu_2]$ can be calculated with

$$C(\tau) = \int_{\nu_1}^{\nu_2} \frac{f_\nu(\tau)}{h\nu} d\nu = \frac{2\pi R_c^2}{hD^2 \Gamma^3 (1 - \beta)^2 \{1 + [\beta/(1 - \beta)]\tau\}^2} \times \int_{\tilde{\tau}_{\theta, \min}}^{\tilde{\tau}_{\theta, \max}} \left[\tilde{I}(\tau_\theta) (1 + \beta\tau_\theta)^2 (1 - \tau + \tau_\theta) \int_{\nu_1}^{\nu_2} \frac{g_{0, \nu}(\nu_{0, \theta})}{\nu} d\nu \right] d\tau_\theta. \quad (2)$$

This suggests that except for the mechanism [i.e., $\tilde{I}(\tau_\theta)$ and $g_{0, \nu}(\nu_{0, \theta})$] and the state of the fireball (i.e., Γ , R_c , and D), light curves of the source depend on the energy range as well.

For the sake of simplicity, we first employ a local pulse to study the relationship in great detail and later employ other local pulses to study the same issue in less detail. The local pulse considered in this section is that of Gaussian that is assumed to be

$$\tilde{I}(\tau_\theta) = I_0 \exp \left[- \left(\frac{\tau_\theta - \tau_{\theta, 0}}{\sigma} \right)^2 \right], \quad \tau_{\theta, \min} \leq \tau_\theta, \quad (3)$$

where I_0 , σ , $\tau_{\theta, 0}$, and $\tau_{\theta, \min}$ are constants. As shown in Paper I, there is a constraint to the lower limit of τ_θ , which is $\tau_{\theta, \min} > -1/\beta$. Due to this constraint, it is impossible to take a negative infinity value of $\tau_{\theta, \min}$, and therefore the interval between $\tau_{\theta, 0}$ and $\tau_{\theta, \min}$ must be limited. Here we assign $\tau_{\theta, 0} = 10\sigma + \tau_{\theta, \min}$ so that the interval between $\tau_{\theta, 0}$ and $\tau_{\theta, \min}$ would be large enough to make the rising part of the local pulse close to that of the Gaussian pulse. The FWHM of the Gaussian pulse is $\Delta\tau_{\theta, \text{FWHM}} = 2(\ln 2)^{1/2}\sigma$, which leads to $\sigma = \Delta\tau_{\theta, \text{FWHM}}/2(\ln 2)^{1/2}$. In the following we assign $\tau_{\theta, \min} = 0$, take $\Delta\tau_{\theta, \text{FWHM}} = 0.01, 0.1, 1$, and 10, and adopt $\Gamma = 10, 100$, and 1000.

2.1. The Case of a Typical Band Function

Here we employ the Band function (Band et al. 1993) with typical indexes $\alpha_0 = -1$ and $\beta_0 = -2.25$ as the rest-frame radiation form to investigate how the FWHM and the FWHM1/FWHM2 are related to the corresponding energy, where FWHM1 and FWHM2 are the FWHMs in the rising and decaying phases of the light curve, respectively. The FWHM and FWHM1/FWHM2 of the observed light curve arising from the local Gaussian pulse associated with certain frequency could be well determined according to equation (2), when equation (3) is applied. Displayed in Figures 1a and 1b are the FWHM- $\nu/\nu_{0, p}$ and FWHM1/FWHM2- $\nu/\nu_{0, p}$ curves, respectively. One finds from these curves that for all sets of the parameters adopted here, a semi-power-law relationship between each of the two quantities (FWHM and FWHM1/FWHM2) and $\nu/\nu_{0, p}$ can be observed within a range (called the power-law range) spanning more than 1 order of magnitude in frequency. Beyond this range (i.e., in higher and lower frequency bands), both the FWHM and FWHM1/FWHM2 of the observed light curve remains unchanged with frequency. We call the unchanged section of the curves in the lower frequency band relative to the power-law range the “lower band plateau” and that in the higher frequency band the “higher band plateau.” For a certain rest-frame spectrum (say, when the value of $\nu_{0, p}$ is fixed), the power-law range shifts to higher energy bands when Γ becomes larger. The power-law range could therefore become an indicator of the Lorentz factor as long as $\nu_{0, p}$ is fixed (in practice, as $\nu_{0, p}$ is always unclear, what can be determined is the product $\Gamma\nu_{0, p}$, which is directly associated with the observed peak energy E_p ; see discussion below).

The power-law range shown in an FWHM- $\nu/\nu_{0, p}$ curve is marked by a smooth turning at its lower energy end and a sharp turning at its higher end. Let ν_{low} (or E_{low}) denote the position of the turning at the lower energy end and ν_{high} (or E_{high}) represent that at the higher end. One finds that ν_{high} is well defined due to the sharp feature associated with it while ν_{low} is not since the corresponding feature is smooth. Following to Figure 1a, we simply define ν_{low} by $\log \text{FWHM}(\nu_{\text{low}}) \equiv \log \text{FWHM}_{\text{max}} - (\log \text{FWHM}_{\text{max}} - \log \text{FWHM}_{\text{min}})/10$, where FWHM_{min} and FWHM_{max} are the minimum and maximum values of the FWHM of the light curves. Listed in Table 1 are the values of ν_{low} and ν_{high} as well as FWHM_{min} and FWHM_{max} deduced from the curves of Figure 1a. One can conclude from this table that $\nu_{\text{high}} \simeq (2.4-2.5)\Gamma\nu_{0, p}$ for all the adopted Lorentz factors ($\Gamma = 10, 100$, and 1000) and that $\log \nu_{\text{high}} - \log \nu_{\text{low}} \simeq 1.19-1.26, 1.20-1.25$, and 1.20-1.26 for $\Gamma = 10, 100$, and 1000, respectively. This reveals that ν_{high} is proportional to $\Gamma\nu_{0, p}$. For the same value of $\Gamma\nu_{0, p}$, ν_{high} is independent of Γ or $\nu_{0, p}$. The power-law range spans more than 1 order of magnitude in frequency for all the Lorentz factors concerned. In addition, we find that for the same value of $\Delta\tau_{\theta, \text{FWHM}}$, $\text{FWHM}_{\text{min}} \propto \Gamma^{-2}$ and $\text{FWHM}_{\text{max}} \propto \Gamma^{-2}$.

As shown in Qin (2002), when taking into account the Doppler effect of fireballs, the observed peak frequency is related

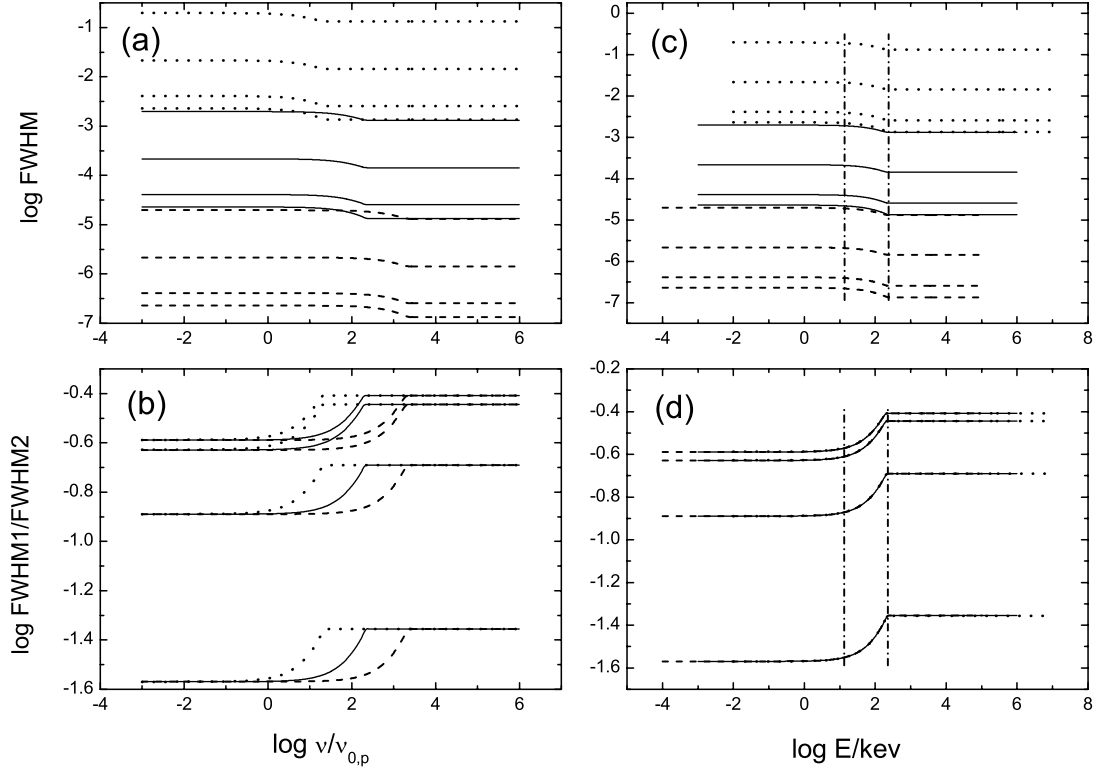


FIG. 1.—Relationships between (a) the FWHM and energy and (b) the ratio FWHM1/FWHM2 and energy for the light curve of eq. (2) confined within $0.99\nu/\nu_{0,p} \leq \nu/\nu_{0,p} \leq 1.01\nu/\nu_{0,p}$, in the case of adopting the Band function with $\alpha_0 = -1$ and $\beta_0 = -2.25$ as the rest-frame radiation form and the Gaussian pulse as its local pulse. Dotted lines from bottom to top represent the curves associated with $\Delta\tau_{\theta,\text{FWHM}} = 0.01, 0.1, 1$, and 10 for $\Gamma = 10$; solid lines from bottom to top represent the curves associated with $\Delta\tau_{\theta,\text{FWHM}} = 0.01, 0.1, 1$, and 10 for $\Gamma = 1000$. Shown in (c) and (d) are the curves in (a) and (b), respectively, where the corresponding energy is presented in units of keV. The two vertical dash-dotted lines in (c) and (d) denote the power-law ranges deduced from the curves associated with the case of $(\Gamma, \Delta\tau_{\theta,\text{FWHM}}) = (100, 10)$.

to the peak frequency of the typical rest-frame Band function spectrum by $\nu_p \simeq 1.67\Gamma\nu_{0,p}$, i.e., $E_p \simeq 1.67\Gamma E_{0,p}$. In terms of E_p , we get from Table 1 that $\log E_{\text{low}} - \log E_p \simeq -1.10$ to -1.02 and $\log E_{\text{high}} - \log E_p \simeq 0.157$ to 0.177 .

In the same way, we confine the power-law range shown in Figure 1b with ν_{low} and ν_{high} as well, with ν_{low} being defined by $\log(\text{FWHM1}/\text{FWHM2})(\nu_{\text{low}}) \equiv \log(\text{FWHM1}/\text{FWHM2})_{\text{min}} + [\log(\text{FWHM1}/\text{FWHM2})_{\text{max}} - \log(\text{FWHM1}/\text{FWHM2})_{\text{min}}]/10$. Listed in Table 2 are the values of ν_{low} , ν_{high} , $(\text{FWHM1}/\text{FWHM2})_{\text{min}}$, and $(\text{FWHM1}/\text{FWHM2})_{\text{max}}$ obtained from the curves of Figure 1b. We find from this table that $\nu_{\text{high}} \simeq (2.3 -$

$2.4)\Gamma\nu_{0,p}$, $(2.3-2.5)\Gamma\nu_{0,p}$, and $(2.2-2.5)\Gamma\nu_{0,p}$ for $\Gamma = 10, 100$, and 1000 , respectively, and $\log \nu_{\text{high}} - \log \nu_{\text{low}} \simeq 1.18-1.25$, $1.20-1.24$, and $1.20-1.25$ for $\Gamma = 10, 100$, and 1000 , respectively. This also shows that although both ν_{high} and ν_{low} are proportional to $\Gamma\nu_{0,p}$, they are independent of Γ or $\nu_{0,p}$ alone. In terms of E_p , we get $\log E_{\text{low}} - \log E_p \simeq -1.10$ to -1.02 and $\log E_{\text{high}} - \log E_p \simeq 0.127$ to 0.167 . In addition, we find that for the same value of $\Delta\tau_{\theta,\text{FWHM}}$, $\text{FWHM}_{\text{min}} \propto \Gamma^{-2}$ and $\text{FWHM}_{\text{max}} \propto \Gamma^{-2}$. Table 2 suggests that the values of $(\text{FWHM1}/\text{FWHM2})_{\text{min}}$ and $(\text{FWHM1}/\text{FWHM2})_{\text{max}}$ rely only on the local pulse width $\Delta\tau_{\theta,\text{FWHM}}$.

TABLE 1
TURNING FREQUENCY AND TYPICAL WIDTH OBTAINED
FROM THE CURVES IN FIGURE 1a

Γ	$\Delta\tau_{\theta,\text{FWHM}}$	$\log \frac{\nu_{\text{low}}}{\nu_{0,p}}$	$\log \frac{\nu_{\text{high}}}{\nu_{0,p}}$	$\log \text{FWHM}_{\text{min}}$	$\log \text{FWHM}_{\text{max}}$
10.....	0.01	0.20	1.39	-2.87	-2.64
	0.1	0.17	1.38	-2.59	-2.39
	1	0.13	1.38	-1.84	-1.66
	10	0.12	1.38	-0.88	-0.71
100.....	0.01	1.20	2.40	-4.87	-4.64
	0.1	1.17	2.40	-4.59	-4.39
	1	1.14	2.38	-3.84	-3.66
	10	1.13	2.38	-2.88	-2.71
1000.....	0.01	2.20	3.40	-6.87	-6.64
	0.1	2.18	3.39	-6.59	-6.39
	1	2.14	3.38	-5.84	-5.66
	10	2.13	3.39	-4.88	-4.71

TABLE 2
TURNING FREQUENCY AND TYPICAL WIDTH OBTAINED
FROM THE CURVES IN FIGURE 1b

Γ	$\Delta\tau_{\theta,\text{FWHM}}$	$\log \frac{\nu_{\text{low}}}{\nu_{0,p}}$	$\log \frac{\nu_{\text{high}}}{\nu_{0,p}}$	$\log(\frac{\text{FWHM1}}{\text{FWHM2}})_{\text{min}}$	$\log(\frac{\text{FWHM1}}{\text{FWHM2}})_{\text{max}}$
10.....	0.01	0.20	1.38	-1.57	-1.36
	0.1	0.16	1.37	-0.89	-0.69
	1	0.13	1.37	-0.63	-0.44
	10	0.12	1.37	-0.59	-0.41
100.....	0.01	1.19	2.39	-1.57	-1.35
	0.1	1.16	2.36	-0.89	-0.69
	1	1.13	2.36	-0.63	-0.44
	10	1.12	2.36	-0.59	-0.41
1000.....	0.01	2.19	3.39	-1.57	-1.35
	0.1	2.16	3.36	-0.89	-0.69
	1	2.13	3.35	-0.63	-0.44
	10	2.12	3.37	-0.59	-0.41

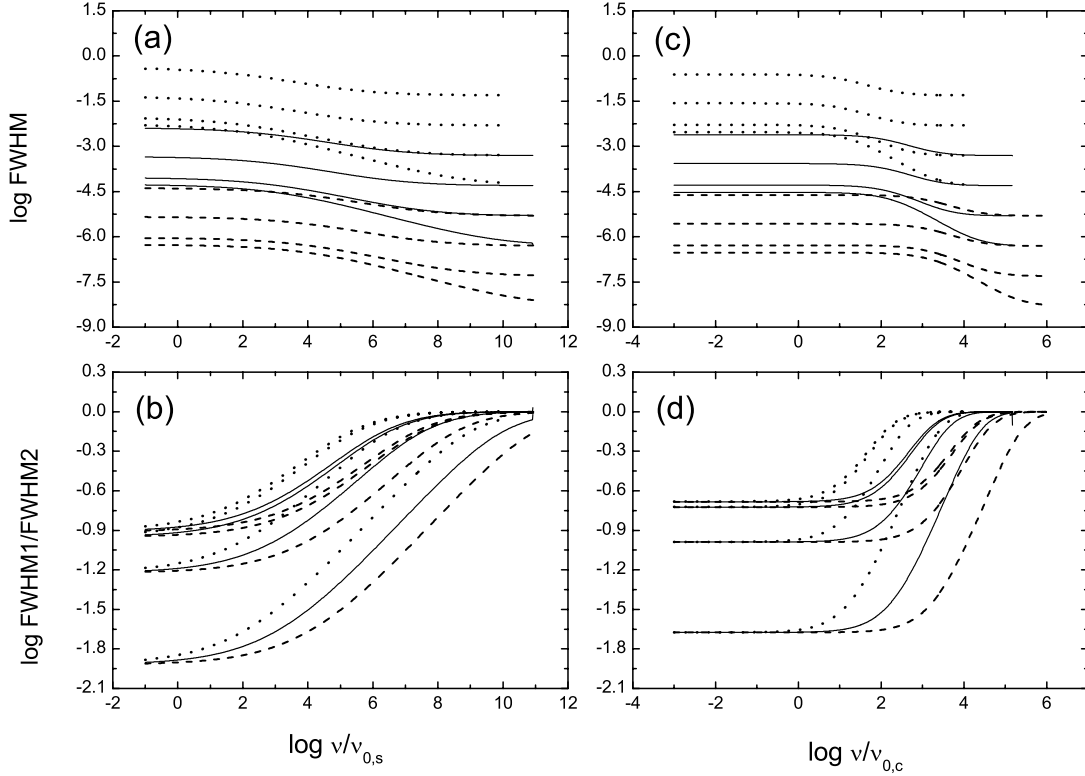


FIG. 2.—Relationships between the FWHM and FWHM1/FWHM2 of pulses, on one hand, and energy, on the other, for light curve of eq. (2) confined within $0.99\nu/\nu_{0,p} \leq \nu/\nu_{0,p} \leq 1.01\nu/\nu_{0,p}$, in the case of adopting the thermal synchrotron spectrum (left) and Comptonized spectrum (right) as the rest-frame radiation form and the Gaussian pulse as its local pulse. Dotted lines from bottom to top represent the curves associated with $\Delta\tau_{\theta,\text{FWHM}} = 0.01, 0.1, 1$, and 10 for $\Gamma = 10$; solid lines from bottom to top represent the curves associated with $\Delta\tau_{\theta,\text{FWHM}} = 0.01, 0.1, 1$, and 10 for $\Gamma = 100$; dashed lines from bottom to top stand for the curves associated with $\Delta\tau_{\theta,\text{FWHM}} = 0.01, 0.1, 1$, and 10 for $\Gamma = 1000$.

The relation between E_{low} and E_p or between E_{high} and E_p suggests that once we obtain the value of E_{low} or E_{high} in the case of the typical rest-frame Band function spectrum, we should be able to estimate E_p , or vice versa.

We notice that a certain value of $\nu/\nu_{0,p}$ might correspond to different energies associated with different values of $\nu_{0,p}$. Let us assign $\nu_{0,p} = 10 \text{ keV } h^{-1}$ when taking $\Gamma = 10$, $\nu_{0,p} = 1 \text{ keV } h^{-1}$ when taking $\Gamma = 100$, and $\nu_{0,p} = 0.1 \text{ keV } h^{-1}$ when taking $\Gamma = 1000$. In this situation, $\Gamma\nu_{0,p} = 100 \text{ keV } h^{-1}$ holds for all these cases. Figure 1c shows the curves of Figure 1a in terms of energy, where the power-law range confined by $\log E_{\text{low}}/\text{keV} = 1.13$ and $\log E_{\text{high}}/\text{keV} = 2.38$ (see Table 1) is displayed. Figure 1d shows the curves of Figure 1b in terms of energy, where the power-law range confined by $\log E_{\text{low}}/\text{keV} = 1.12$ and $\log E_{\text{high}}/\text{keV} = 2.36$ (see Table 2) is plotted. From Figure 1d, one finds that the curves corresponding to $\Gamma = 10, 100$, and 1000 are difficult to distinguish. When the values of $\Gamma\nu_{0,p}$ are the same (here $\Gamma\nu_{0,p} = 100 \text{ keV } h^{-1}$), the two relationships (one is between FWHM and energy, and the other is between FWHM1/FWHM2 and energy) are independent of the Lorentz factor, and the power-law ranges of the curves arising from $\Gamma = 10, 100$, and 1000 become almost the same.

One can conclude from this analysis that in the case of adopting the typical Band function with $\alpha_0 = -1$ and $\beta_0 = -2.25$ as the rest-frame radiation form, there exists a semi-power-law relationship spanning more than 1 order of magnitude in energy between the width of pulses and energy, as well as between the ratio of the rising width to the decaying width of pulses and energy. The upper and lower limits of this power-law range are well related to the observed peak energy E_p of a fireball source.

2.2. The Case of Other Spectra

Let us consider as the rest-frame radiation form two other spectra that are much different from the Band function (especially in the high-energy band). One is the thermal synchrotron spectrum, $I_\nu \propto (\nu/\nu_{0,s}) \exp [-(\nu/\nu_{0,s})^{1/3}]$, where $\nu_{0,s}$ is a constant including all constants in the exponential index (Liang et al. 1983). The other is the Comptonized spectrum, $I_\nu \propto \nu^{1+\alpha_{0,C}} \exp (-\nu/\nu_{0,C})$, where $\alpha_{0,C}$ and $\nu_{0,C}$ are constants. A typical value $\alpha_{0,C} = -0.6$ (Schaefer et al. 1994) for the index of the Comptonized radiation will be adopted.

Figures 2a and 2b show the FWHM- $\nu/\nu_{0,s}$ and FWHM1/FWHM2- $\nu/\nu_{0,s}$ curves, respectively, corresponding to the rest-frame thermal synchrotron spectrum and local Gaussian pulse (eq. [3]). A semi-power-law relationship can also be observed in both plots. In the case of $\Delta\tau_{\theta,\text{FWHM}} = 1$ (where the turnover is well defined in the two plots), we get from Figure 2a that $\nu_{\text{high}} \simeq 1.6 \times 10^5 \Gamma\nu_{0,s}$, $1.7 \times 10^5 \Gamma\nu_{0,s}$, and $1.7 \times 10^5 \Gamma\nu_{0,s}$ for $\Gamma = 10, 100$, and 1000 , respectively, and that $\log \nu_{\text{high}} - \log \nu_{\text{low}} \simeq 5.30, 5.53$, and 5.66 for $\Gamma = 10, 100$, and 1000 , respectively, and we obtain from Figure 2b that $\nu_{\text{high}} \simeq 4.6 \times 10^5 \Gamma\nu_{0,s}$, $4.8 \times 10^5 \Gamma\nu_{0,s}$, and $4.7 \times 10^5 \Gamma\nu_{0,s}$ for $\Gamma = 10, 100$, and 1000 , respectively, and that $\log \nu_{\text{high}} - \log \nu_{\text{low}} \simeq 5.75, 5.99$, and 6.09 for $\Gamma = 10, 100$, and 1000 , respectively. This suggests that in the case of the rest-frame thermal synchrotron spectrum, ν_{high} is proportional to $\Gamma\nu_{0,s}$ and that the power-law range can span more than 5 orders of magnitude in frequency.

Shown in Figures 2c and 2d are the FWHM- $\nu/\nu_{0,p}$ and FWHM1/FWHM2- $\nu/\nu_{0,p}$ curves, respectively, associated with the rest-frame Comptonized spectrum and arising from the local

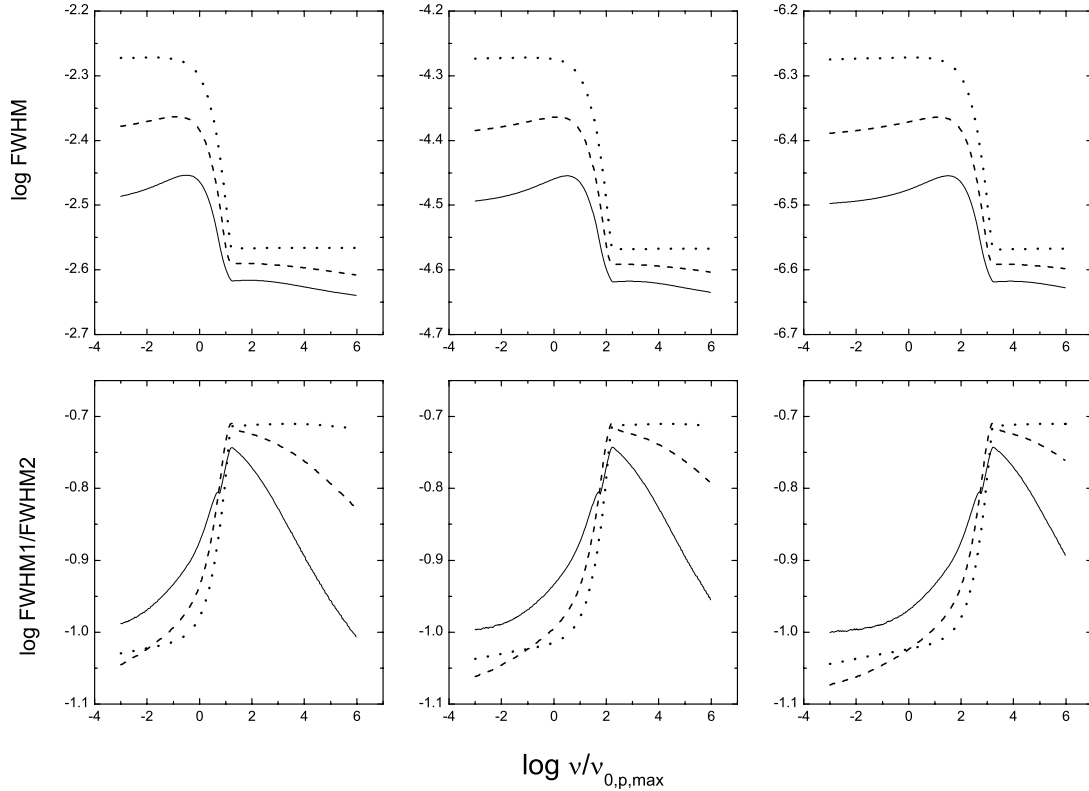


FIG. 3.—Relationships between the FWHM of pulses and energy (*top*) and between FWHM1/FWHM2 and energy (*bottom*) for the light curve of eq. (2) confined within $0.99\nu/\nu_{0,p} \leq \nu/\nu_{0,p} \leq 1.01\nu/\nu_{0,p}$ in the case of adopting the varying Band function (see § 2.3) as the rest-frame radiation form and the Gaussian pulse of eq. (3) with $\Delta\tau_{\theta,\text{FWHM}} = 0.1$ as its local pulse, for $\Gamma = 10$ (left), 100 (middle), and 1000 (right), where $\nu_{0,p,\max} = 10^{0.1}$. The dotted, dashed, and solid lines represent the curves with $k = 0.1, 0.5$, and 1.0 , respectively.

Gaussian pulse (eq. [3]). A semi–power-law relationship can also be detected in both plots. In the case of $\Delta\tau_{\theta,\text{FWHM}} = 1$ we deduce from Figure 2c that $\nu_{\text{high}} \simeq 1.2 \times 10^2 \Gamma \nu_{0,C}$, $1.2 \times 10^2 \Gamma \nu_{0,C}$, and $1.3 \times 10^2 \Gamma \nu_{0,C}$ for $\Gamma = 10, 100$, and 1000 , respectively, and that $\log \nu_{\text{high}} - \log \nu_{\text{low}} \simeq 2.44, 2.45$, and 2.46 for $\Gamma = 10, 100$, and 1000 , respectively, and we find from Figure 2d that $\nu_{\text{high}} \simeq 1.2 \times 10^2 \Gamma \nu_{0,C}$, $1.1 \times 10^2 \Gamma \nu_{0,C}$, and $1.2 \times 10^2 \Gamma \nu_{0,C}$ for $\Gamma = 10, 100$, and 1000 , respectively, and that $\log \nu_{\text{high}} - \log \nu_{\text{low}} \simeq 2.45, 2.43$, and 2.45 for $\Gamma = 10, 100$, and 1000 , respectively. In the case of the rest-frame Comptonized spectrum, ν_{high} is proportional to $\Gamma \nu_{0,C}$. The power-law range spans more than 2 orders of magnitude in frequency.

We conclude that in the case of adopting a rest-frame spectrum with an exponential tail in the high-energy band, a semi–power-law relationship between the FWHM and energy or between FWHM1/FWHM2 and energy can also be observed. The range (spanning over more than 2 orders of magnitude in energy) is much larger than in the case of the Band function. It seems common that for a rest-frame spectrum, there exists a power-law relationship between each of the FWHM and FWHM1/FWHM2 and energy within an energy range. The range is very sensitive to the rest-frame spectrum and the product of the rest-frame peak energy and the Lorentz factor.

2.3. The Case of the Rest-Frame Radiation Form Varying with Time

It is known that the indexes of the spectra of many GRBs vary with time (see Preece et al. 2000). We are curious as to what the relationship is if the rest-frame spectrum develops with time. Here, corresponding to the soft-to-hard phenomenon, let us consider a simple case where the rest-frame spectrum is a Band function

with its indexes and the peak frequency decreasing with time. We assume a simple evolution of indexes α_0 and β_0 and peak frequency $\nu_{0,p}$ that follows $\alpha_0 = -0.5 - k(\tau_{\theta} - \tau_{\theta,1})/(\tau_{\theta,2} - \tau_{\theta,1})$, $\beta_0 = -2 - k(\tau_{\theta} - \tau_{\theta,1})/(\tau_{\theta,2} - \tau_{\theta,1})$, and $\log \nu_{0,p} = 0.1 - k(\tau_{\theta} - \tau_{\theta,1})/(\tau_{\theta,2} - \tau_{\theta,1})$ for $\tau_{\theta,1} \leq \tau_{\theta} \leq \tau_{\theta,2}$. For $\tau_{\theta} < \tau_{\theta,1}$, $\alpha_0 = -0.5$, $\beta_0 = -2$, and $\log \nu_{0,p} = 0.1$, while for $\tau_{\theta} > \tau_{\theta,2}$, $\alpha_0 = -0.5 - k$, $\beta_0 = -2 - k$, and $\log \nu_{0,p} = 0.1 - k$. We take $k = 0.1, 0.5$, and 1 (these correspond to different rates of decrease) and adopt $\Gamma = 10, 100, 1000$, respectively, in the following analysis.

Let us employ the local Gaussian pulse of equation (3) with $\Delta\tau_{\theta,\text{FWHM}} = 0.1$ to study the relationship. We adopt $\tau_{\theta,1} = 9\sigma + \tau_{\theta,\min}$ and $\tau_{\theta,2} = 11\sigma + \tau_{\theta,\min}$ and once more assign $\tau_{\theta,0} = 10\sigma + \tau_{\theta,\min}$ and $\tau_{\theta,\min} = 0$ (see above). Figure 3 displays the expected FWHM- $\nu/\nu_{0,p,\max}$ and FWHM1/FWHM2- $\nu/\nu_{0,p,\max}$ curves, where the frequency is presented in units of $\nu_{0,p,\max}$, which is the largest value of $\nu_{0,p}$ adopted.

We find that when the rate of decrease becomes larger (say, $k = 0.5$ or 1), the relationships obviously differ from what was noticed above. In this situation, the relationship between the pulse width and energy shows at least two semi–power-law ranges with the index in the lower energy band being positive, and therefore a peak value of the width marking the two lower energy power-law ranges is observed. Accordingly, the lower band plateau noted above disappears. In the case of the relationship between FWHM1/FWHM2 and ν , a peak of FWHM1/FWHM2 marking two higher energy semi–power-law ranges is also detected. This peaked feature is a remarkable signature of the evolution of the rest-frame spectrum.

2.4. The Case of Other Local Pulses

Here we investigate whether different local pulses lead to a very different result. Three forms of local power-law pulses are

considered. We choose power-law forms instead of other local pulse forms due to the fact that different values of the power-law index correspond to entirely different forms of local pulses.

The first is the local pulse with a power-law rise and a power-law decay, which is assumed to be

$$\tilde{I}(\tau_\theta) = I_0 \begin{cases} \left(\frac{\tau_\theta - \tau_{\theta,\min}}{\tau_{\theta,0} - \tau_{\theta,\min}} \right)^\mu, & \tau_{\theta,\min} \leq \tau_\theta \leq \tau_{\theta,0}, \\ \left(1 - \frac{\tau_\theta - \tau_{\theta,0}}{\tau_{\theta,\max} - \tau_{\theta,0}} \right)^\mu, & \tau_{\theta,0} < \tau_\theta \leq \tau_{\theta,\max}, \end{cases} \quad (4)$$

where I_0 , μ , $\tau_{\theta,\min}$, $\tau_{\theta,0}$, and $\tau_{\theta,\max}$ are constants. The peak of this intensity is at $\tau_{\theta,0}$, and the two FWHM positions of this intensity before and after $\tau_{\theta,0}$ are $\tau_{\theta,\text{FWHM1}} = 2^{-1/\mu}\tau_{\theta,0} + (1 - 2^{-1/\mu})\tau_{\theta,\min}$ and $\tau_{\theta,\text{FWHM2}} = 2^{-1/\mu}\tau_{\theta,0} + (1 - 2^{-1/\mu})\tau_{\theta,\max}$, respectively. In the case of $\mu = 2$, the FWHM of this local pulse is $\Delta\tau_{\theta,\text{FWHM}} = (1 - 1/\sqrt{2})(\tau_{\theta,\max} - \tau_{\theta,\min})$, which leads to $\tau_{\theta,\max} = \Delta\tau_{\theta,\text{FWHM}}/(1 - 1/\sqrt{2}) + \tau_{\theta,\min}$. The second is the local pulse with a power-law rise, which is written as

$$\tilde{I}(\tau_\theta) = I_0 \left(\frac{\tau_\theta - \tau_{\theta,\min}}{\tau_{\theta,\max} - \tau_{\theta,\min}} \right)^\mu, \quad \tau_{\theta,\min} \leq \tau_\theta \leq \tau_{\theta,\max}. \quad (5)$$

The peak of this intensity is at $\tau_{\theta,\max}$. In the case of $\mu = 2$, the relation of $\tau_{\theta,\max} = \Delta\tau_{\theta,\text{FWHM}}/(1 - 1/\sqrt{2}) + \tau_{\theta,\min}$ holds. The third is the local pulse with a power-law decay that follows

$$\tilde{I}(\tau_\theta) = I_0 \left(1 - \frac{\tau_\theta - \tau_{\theta,\min}}{\tau_{\theta,\max} - \tau_{\theta,\min}} \right)^\mu, \quad \tau_{\theta,\min} < \tau_\theta \leq \tau_{\theta,\max}. \quad (6)$$

The peak of this intensity is at $\tau_{\theta,\min}$. In the case of $\mu = 2$, the relation of $\tau_{\theta,\max} = \Delta\tau_{\theta,\text{FWHM}}/(1 - 1/\sqrt{2}) + \tau_{\theta,\min}$ holds as well.

We assign $\tau_{\theta,\min} = 0$ and $\mu = 2$ and take $\Delta\tau_{\theta,\text{FWHM}} = 0.01, 0.1, 1$, and 10 , $\Gamma = 10, 100, 1000$, $\alpha_0 = -1$, and $\beta_0 = -2.25$ to study the width of light curves arising from these forms of local pulses. For the local pulse given by equation (4), we adopt $\tau_{\theta,0} = \tau_{\theta,\max}/2$.

We find in the FWHM- $\nu/\nu_{0,p}$ and FWHM1/FWHM2- $\nu/\nu_{0,p}$ plots (which are omitted due to the similarity to Fig. 1) associated with the local pulse given by equation (4) that a semi-power-law relationship between each of the two pulse width quantities and frequency is also observed for all sets of the adopted parameters. The power-law range of frequency is quite similar to that in the case of the local Gaussian pulse. The only significant differences are that (1) the magnitude of the width of the expected light curve is much smaller than in the case of the local Gaussian pulse if the local pulse width is sufficiently large (when the local pulse width is small enough, the observed width of the light curve differs slightly), and that (2) the magnitude of the ratio of widths of the corresponding light curve is much larger than in the case of the local Gaussian pulse, regardless how large the local pulse width is. From the FWHM- $\nu/\nu_{0,p}$ curves we find that for all the adopted values of the Lorentz factor ($\Gamma = 10, 100$, and 1000), $\nu_{\text{high}} \simeq (2.4-2.5)\Gamma\nu_{0,p}$, and for $\Gamma = 10, 100$, and 1000 , $\log \nu_{\text{high}} - \log \nu_{\text{low}} \simeq 1.19-1.38, 1.19-1.38$, and $1.20-1.38$, respectively. From the FWHM1/FWHM2- $\nu/\nu_{0,p}$ curves we get $\nu_{\text{high}} \simeq (1.7-2.6)\Gamma\nu_{0,p}$, $(1.8-2.5)\Gamma\nu_{0,p}$, and $(1.8-2.5)\Gamma\nu_{0,p}$ for $\Gamma = 10, 100$, and 1000 , respectively, and $\log \nu_{\text{high}} - \log \nu_{\text{low}} \simeq 1.21-1.37, 1.20-1.39$, and $1.20-1.38$ for $\Gamma = 10, 100$, and 1000 , respectively. The values of $(\text{FWHM1}/\text{FWHM2})_{\min}$ and $(\text{FWHM1}/\text{FWHM2})_{\max}$ rely only on the local pulse width $\Delta\tau_{\theta,\text{FWHM}}$, being independent of the Lorentz factor. Thus, the conclusion obtained

in the case of the local Gaussian pulse holds when adopting the local pulse given by equation (4).

Adopting the local pulse given by equation (5), one obtains similar results. We find from the relationship between the width of pulses and frequency that $\nu_{\text{high}} \simeq (2.3-2.5)\Gamma\nu_{0,p}$, $(2.4-2.5)\Gamma\nu_{0,p}$, and $(2.4-2.5)\Gamma\nu_{0,p}$ for $\Gamma = 10, 100$, and 1000 , respectively, and $\log \nu_{\text{high}} - \log \nu_{\text{low}} \simeq 1.19-1.26, 1.19-1.28$, and $1.20-1.28$ for $\Gamma = 10, 100$, and 1000 , respectively. In addition, we get from the relationship between the ratio of widths FWHM1/FWHM2 and frequency that $\nu_{\text{high}} \simeq 2.5\Gamma\nu_{0,p}$, $2.5\Gamma\nu_{0,p}$, and $(2.5-2.6)\Gamma\nu_{0,p}$ for $\Gamma = 10, 100$, and 1000 , respectively, and $\log \nu_{\text{high}} - \log \nu_{\text{low}} \simeq 1.20-1.26, 1.20-1.25$, and $1.20-1.25$ for $\Gamma = 10, 100$, and 1000 , respectively. In the same way, we get similar results when adopting the local pulse given by equation (6). From the relationship between the width of pulses and frequency, we obtain $\nu_{\text{high}} \simeq (2.3-2.5)\Gamma\nu_{0,p}$, $(2.4-2.5)\Gamma\nu_{0,p}$, and $(2.4-2.5)\Gamma\nu_{0,p}$ for $\Gamma = 10, 100$, and 1000 , respectively, and $\log \nu_{\text{high}} - \log \nu_{\text{low}} \simeq 1.19-1.39, 1.20-1.48$, and $1.20-1.47$ for $\Gamma = 10, 100$, and 1000 , respectively. From the relationship between the ratio of widths and frequency we find $\nu_{\text{high}} \simeq (2.0-2.4)\Gamma\nu_{0,p}$, $(2.0-2.4)\Gamma\nu_{0,p}$, and $(2.1-2.4)\Gamma\nu_{0,p}$ for $\Gamma = 10, 100$, and 1000 , respectively, and $\log \nu_{\text{high}} - \log \nu_{\text{low}} \simeq 1.19-1.49, 1.19-1.51$, and $1.19-1.52$ for $\Gamma = 10, 100$, and 1000 , respectively. In both cases, the values of $(\text{FWHM1}/\text{FWHM2})_{\min}$ and $(\text{FWHM1}/\text{FWHM2})_{\max}$ are independent of the Lorentz factor as well, relying only on the local pulse width $\Delta\tau_{\theta,\text{FWHM}}$.

We come to the conclusion that a power-law relationship between each of the two pulse width quantities and frequency is observed in light curves arising from different local pulse forms. The power-law range is not significantly influenced by the local pulse form, but the magnitudes of the width and the ratio of widths are obviously affected.

3. THE RELATIONSHIP EXPECTED FOR TYPICAL HARD AND SOFT BURSTS

As suggested by observation, the value of E_p of bright GRBs is mainly distributed within 100–600 keV (see Preece et al. 2000). According to the above analysis, the power-law range of many bright GRBs is within the energy range covering the four BATSE channels, and this power-law relationship was detected by many authors. However, for this kind of burst, the power-law relationship would fail in the energy range of *Swift*, or there would be a turnover in the relationship within this energy range, assuming that the typical Band function radiation form could approximately be applicable. Here we analyze the relationship between the quantities discussed above in the energy range covering both the BATSE and *Swift* channels for some typical GRBs. The bursts concerned are the so-called hard and soft bursts, which are defined as GRBs with peak energy E_p located above and below the second BATSE channel, $E_p > 100$ keV and $E_p < 50$ keV, respectively. According to this definition, most of bright bursts belong to hard bursts, and according to Strohmayer et al. (1998), many *Ginga* bursts are soft ones.

Assume that typical hard and soft bursts differ only by the Lorentz factor of the expanding motion of the fireball surface. As $E_p \propto \Gamma$ (see Qin 2002), taking $E_p = 250$ keV as a typical value of the peak energy for hard bursts (see Preece et al. 2000) and assigning $\Gamma = 200$ to be the Lorentz factor of these sources, one finds the typical value of the peak energy of a soft burst with $\Gamma = 20$ to be $E_p = 25$ keV, which is well within the range of soft GRBs defined above.

The energy range with which we are concerned here, which covers both BATSE and *Swift*, is divided into the following eight channels: $[E_1, E_2] = [1, 2]$ keV (channel A), $[2, 5]$ keV (channel B),

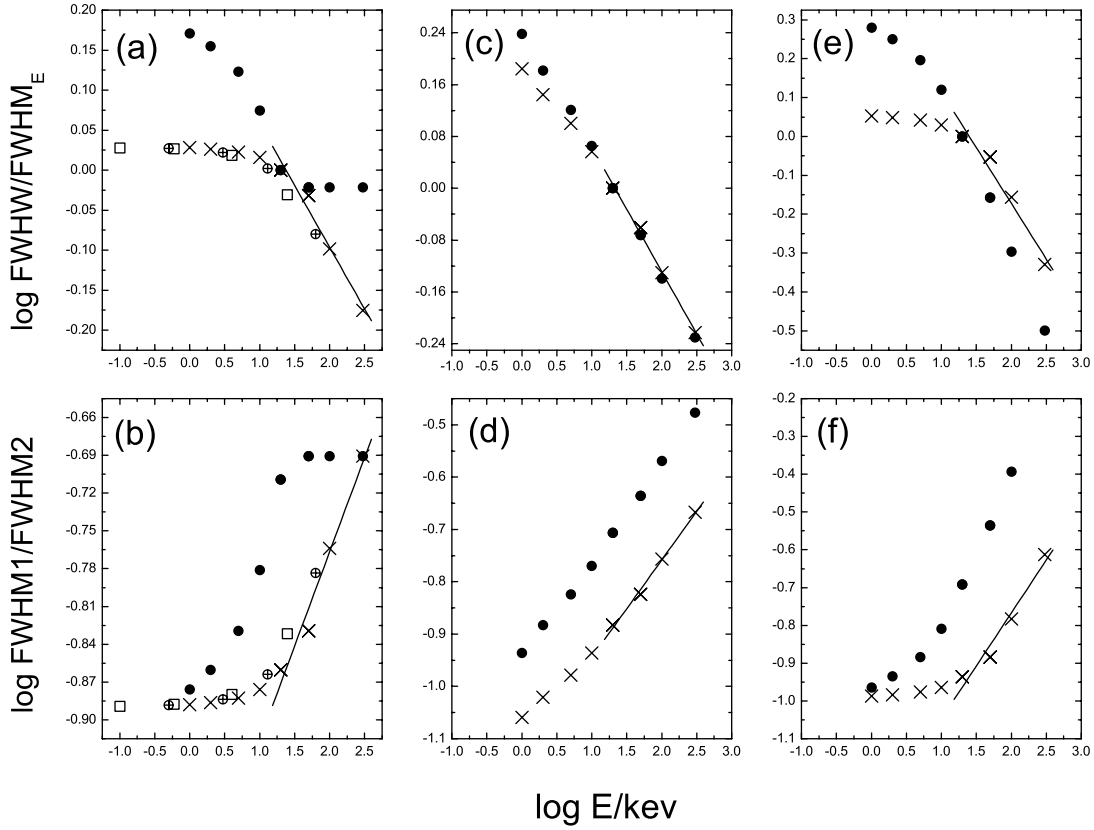


FIG. 4.—Prediction of the relationships between the width of pulses and energy (*top*) and between the ratio of the FWHM of the rising portion to that of the decaying phase of the light curve of pulses, on one hand, and energy, on the other (*bottom*), for the typical hard (*crosses*) and soft (*filled circles*) bursts. The widths are deduced from the light curve of eq. (2) associated with the local Gaussian pulse and the rest-frame Band function with $\alpha_0 = -1$, $\beta_0 = -2.25$, and $\nu_{0,p} = 0.75 \text{ keV } h^{-1}$ (*left*), thermal synchrotron spectrum with $\nu_{0,s} = 3.5 \times 10^{-3} \text{ keV } h^{-1}$ (*middle*), and Comptonized spectrum with $\alpha_{0,C} = -0.6$ and $\nu_{0,C} = 0.55 \text{ keV } h^{-1}$ (*right*), confined within channels A, B, C, D, E, F, G, and H, where we adopt $\Delta\tau_{\theta, \text{FWHM}} = 0.1$ and take $\Gamma = 200$ and $\Gamma = 20$ for typical hard and soft bursts, respectively. The solid line is the power-law curve deduced from the data of the BATSE channels for the typical hard burst. Open squares in left panels represent the expected data of *BeppoSAX*, and open circles filled with pluses stand for those of *HETE-2*.

[5, 10] keV (channel C), [10, 20] keV (channel D), [20, 50] keV (channel E), [50, 100] keV (channel F), [100, 300] keV (channel G), and [300, 1000] keV (channel H). The last four channels are the four BATSE channels.

3.1. Prediction for Various Rest-Frame Radiation Forms

Here we predict the relationship for the typical hard and soft bursts when different rest-frame radiation forms such as the Band function spectrum, thermal synchrotron spectrum, and Comptonized spectrum are involved.

In the case of the Band function, following Qin (2002) we adopt the relation $\nu_p \simeq 1.67\Gamma\nu_{0,p}$. Applying $E_p = 250 \text{ keV}$ and $\Gamma = 200$, we obtain $\nu_{0,p} = 0.75 \text{ keV } h^{-1}$, which will be applied to both the typical hard and soft bursts.

From Preece et al. (2000), we find that the low-energy power-law index of bright bursts is mainly distributed within -2 to 0 and that the high-energy power-law index is distributed mainly within -3.5 to -1.5 . According to Qin (2002), the indexes are not significantly affected by the Doppler effect of fireballs. We therefore consider indexes within these ranges.

We calculate the FWHM and the ratio of the rising width FWHM1 to the decaying width FWHM2 of the eight channels defined above in the case of adopting the rest-frame Band function spectrum with $(\alpha_0, \beta_0) = (-1, -2.25)$ and the local Gaussian pulse with various widths, calculated for both the typical hard ($\Gamma = 200$ and $\nu_{0,p} = 0.75 \text{ keV } h^{-1}$) and soft ($\Gamma = 20$ and $\nu_{0,p} = 0.75 \text{ keV } h^{-1}$) bursts (the corresponding table is omitted).

Displayed in Figures 4a and 4b are the relationships between $\text{FWHM}/\text{FWHM}_E$ and E/keV and between $\text{FWHM1}/\text{FWHM2}$ and E/keV , respectively, in the case in which the local Gaussian pulse with $\Delta\tau_{\theta, \text{FWHM}} = 0.1$ is adopted, where FWHM_E is the width of channel E, which is the first BATSE channel. One finds that in the situation considered here, for the typical hard burst the values of $\text{FWHM}/\text{FWHM}_E$ and $\text{FWHM1}/\text{FWHM2}$ in the first four channels (within the *Swift* range) obviously deviate from the power-law curve determined by the data of the four BATSE channels. For the typical soft burst, the power-law range is no longer in the BATSE band but instead shifts to the *Swift* band. We find that in the case of the typical hard burst, the power-law index deduced from the BATSE channels is within -0.18 to -0.09 .

Presented in Figures 4a and 4b are also the data in both the *BeppoSAX* and *HETE-2* bands. One finds that the relationships in these two bands obey the same laws implied by those in the eight channels adopted above. (Note that the data in the highest energy channel of *BeppoSAX* and the highest energy channel of *HETE-2* are seen to be off the corresponding relationship curves derived from the eight channels, which is due to the wider energy ranges attached to these two channels.)

The FWHM and the ratio $\text{FWHM1}/\text{FWHM2}$ of the eight channels in the case of the rest-frame Band function spectra with $(\alpha_0, \beta_0) = (0, -3.5)$ and $(-1.5, -2)$ for the typical hard and soft bursts, respectively, are also calculated (the tables containing the corresponding values are omitted). We find that for the typical hard burst, the deviation of the data of the low-energy

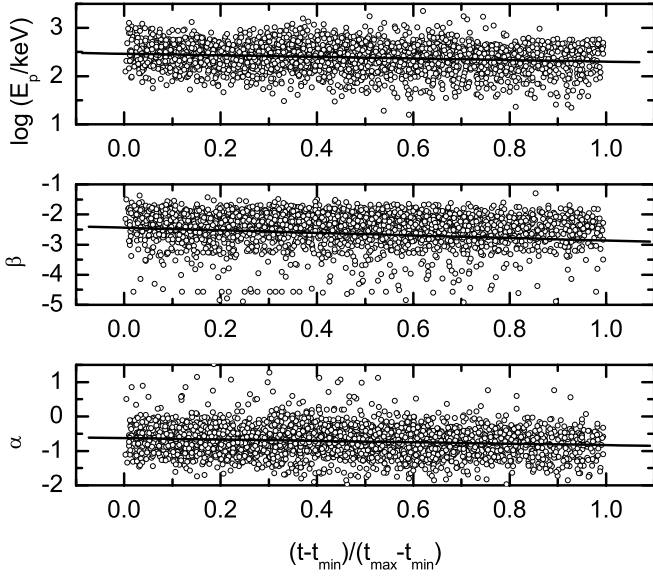


FIG. 5.—Developments of the low- and high-energy indexes and the peak energy of sample 1 in terms of a relative timescale, where t_{\min} and t_{\max} are the lower and the upper limits of the observation time of individual sources. The solid line is the regression line.

Swift channels from the power-law relationship deduced from the data of the four BATSE channels is observed in the two cases considered here. For the typical soft burst, the power-law range is observed in the *Swift* band. In the case of $(\alpha_0, \beta_0) = (0, -3.5)$, the index of the power-law relationship deduced from the four BATSE channels for the typical hard burst ranges from -0.48 to -0.27 , while in the case of $(\alpha_0, \beta_0) = (-1.5, -2)$, the index is confined within -0.07 to -0.03 .

Besides these rest-frame spectra, we have considered several rest-frame Band function spectra with other sets of indexes, and they lead to similar results (the results are omitted).

In the case of the rest-frame thermal synchrotron spectrum, we take $\nu_{0,s} = 3.5 \times 10^{-3} \text{ keV h}^{-1}$ (see Qin 2002, Table 3). Displayed in Figures 4c and 4d are the two relationships in the case of adopting the Gaussian pulse of equation (3) with $\Delta\tau_{\theta, \text{FWHM}} = 0.1$ as the local pulse. We see that for the typical hard burst, both the width and the ratio of the rising to the decaying widths in the lower energy range of *Swift* deviate slightly from the power-law curves obtained from the data from the BATSE channels. For the typical soft burst, the power-law range covers all eight of the channels with which we are concerned, which is very different from the case of the Band function. The most remarkable result is that both the lower and higher band plateaus disappear (for both the typical hard and soft bursts) within these channels. We find that for the typical hard burst, the power-law index deduced from the BATSE channels is within -0.22 to -0.12 .

In the case of the rest-frame Comptonized spectrum (where we adopt $\alpha_{0,C} = -0.6$ as well), we take $\nu_{0,C} = 0.55 \text{ keV h}^{-1}$ (see Qin 2002, Table 2). The relationships in the case of adopting the Gaussian pulse of equation (3) with $\Delta\tau_{\theta, \text{FWHM}} = 0.1$ as the local pulse are presented in Figures 4e and 4f. As shown in these plots, the deviation mentioned above is also observed. The higher band plateaus disappear while the lower ones remain (at least for the typical hard burst) within these channels. For the typical soft burst, the power-law range would span the BATSE channels as well as a few lower energy channels next to them. We find in this situation that for the typical hard burst, the power-law index in the BATSE channels is within -0.32 to -0.18 , while for the

typical soft burst the power-law index in the BATSE channels is within -0.59 to -0.17 .

3.2. Prediction When the Rest-Frame Radiation Form Varies with Time

Here we make our prediction under the assumption that the rest-frame spectrum takes a Band function form with its indexes and peak energy decreasing with time.

In the same way, we assign $\Gamma = 200$ to the typical hard burst and $\Gamma = 20$ to the soft one. The Gaussian pulse of equation (3) with $\Delta\tau_{\theta, \text{FWHM}} = 0.1$ is taken as the local pulse, where we once more assign $\tau_{\theta,0} = 10\sigma + \tau_{\theta, \min}$ and $\tau_{\theta, \min} = 0$.

One finds in Preece et al. (2000) the parameters of the high time resolution spectroscopy of 156 bright GRBs. The Band function model, the broken power law model (including the smoothly broken power law model), and the Comptonized spectral model were employed to fit these sources. Identifying them by the models with which they were fitted, we have three classes, where the class fitted with the Band function contains 95 bursts (sample 1), that of the broken power law includes 55 sources, and that of the Comptonized class has six. We find in sample 1 that statistically, the low- and high-energy indexes α and β and the peak energy E_p of the sources decrease with time. Even for short bursts, this is common. Shown in Figure 5 are the developments of the two indexes and the peak energy for this sample, where a relative timescale $(t - t_{\min})/(t_{\max} - t_{\min})$ is introduced to calculate the relevant correlations. As shown in the figure, the regression line for the low-energy index is $\alpha = -0.63 - 0.20(t - t_{\min})/(t_{\max} - t_{\min})$, that for the high-energy index is $\beta = -2.44 - 0.42(t - t_{\min})/(t_{\max} - t_{\min})$, and that for the peak energy is $\log(E_p/\text{keV}) = 2.46 - 0.16(t - t_{\min})/(t_{\max} - t_{\min})$. As the spectrum observed is not significantly affected by the Doppler effect of fireballs (see Qin 2002), this suggests that the rest-frame radiation form of the sources develops with time as well.

We find from sample 1 that the medians of the distribution of the uncertainty of the three parameters are $\sigma_{E_p} = 33.1 \text{ keV}$,

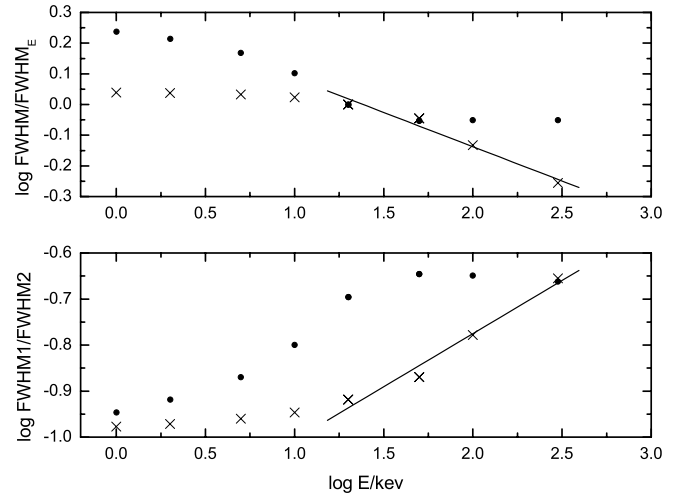


FIG. 6.—Prediction of the relationships between the width of pulses and energy (top) and between the ratio of the FWHM of the rising portion to that of the decaying phase of the light curve of pulses, on one hand, and energy, on the other (bottom), for the typical hard (crosses) and soft (filled circles) bursts in the case where the indexes and the peak energy of the rest-frame Band function spectrum decrease with time. The widths are calculated from light curve of eq. (2) arising from local Gaussian pulse of eq. (3), confined within channels A, B, C, D, E, F, G, and H, where we adopt $\Delta\tau_{\theta, \text{FWHM}} = 0.1$ and take $\Gamma = 200$ and $\Gamma = 20$ for the typical hard and soft bursts, respectively. The solid line is the power-law curve deduced from the data of the BATSE channels for the typical hard burst.

TABLE 3
ESTIMATED VALUES OF THE FWHMS OF THE FOUR BATSE CHANNELS FOR THE 28 GRB SOURCES

Trigger	$W1$	σ_{W1}	$W2$	σ_{W2}	$W3$	σ_{W3}	$W4$	σ_{W4}
907.....	6.791	0.898	3.826	0.338	2.441	0.212
914.....	3.915	0.176	2.562	0.159	1.269	0.350
973.....	7.874	4.530E-6	7.177	0.393	7.072	1.818E-2	5.008	0.360
1406.....	11.375	9.846E-6	9.765	6.605-2	8.041	5.820
1467.....	6.400	0.735	7.053	1.178E-6	5.984	0.569
1733.....	4.989	0.910	4.463	0.454	4.069	0.746	3.308	0.896
1883.....	3.874	0.106	3.288	0.0207	2.585	0.067	1.325	0.053
1956.....	4.920	2.762E-2	4.812	0.326	3.897	0.573
2083.....	3.961	1.675E-4	2.365	1.124	0.892	0.424	0.720	0.206
2102.....	3.488	0.424	4.119	1.001	3.526	0.477
2387.....	18.447	1.295	15.602	1.229	15.085	0.667
2484.....	7.081	2.503	5.241	1.054	4.687	3.200E-2
2665.....	7.205	0.312	5.814	0.367	4.391	0.409
2880.....	1.319	3.360E-2	1.365	9.737E-2	1.150	2.748E-2
2919.....	4.257	8.533E-2	3.714	0.502	2.906	0.942	1.045	0.429
3143.....	2.238	0.329	1.908	2.617	1.334	0.101
3155.....	0.925	0.592	1.229	1.280	1.044	0.302
3870.....	1.842	2.419E-2	2.312	1.514E-2	1.336	1.264E-2
3875.....	0.759	1.751E-2	1.088	0.111	0.592	0.367
3886.....	0.954	3.857E-2	0.661	5.198E-2	0.666	8.197E-2
3892.....	2.979	2.973E-2	1.609	0.180	1.383	0.185
3954.....	2.962	1.125	2.533	0.577	2.602	0.379	0.941	0.0860
4157.....	5.368	1.149	4.209	0.470	1.014	5.743E-2
5478.....	5.052	0.680	6.267	0.251	4.246	0.190
5495.....	1.929	3.197E-4	1.740	2.940E-2	1.096	9.084E-2
5517.....	3.004	1.032	3.146	1.296	2.156	5.173E-2
5523.....	3.877	5.971E-2	4.257	0.488	3.028	2.176E-2
5541.....	4.420	6.866E-2	3.744	1.090	4.862	5.372E-2

NOTE.— $W1$, $W2$, $W3$, and $W4$ are the FWHMs of pulses in the first (20–50 keV), second (50–100 keV), third (100–300 keV), and fourth (>300 keV) energy channels of BATSE, respectively.

$\sigma_\alpha = 0.136$, and $\sigma_\beta = 0.196$, while the medians of the distribution of the deviation (in absolute values) of the data from the regression lines deduced above for the three parameters are $|\Delta E_p| = 97.0$ keV, $|\Delta\alpha| = 0.297$, and $|\Delta\beta| = 0.410$. This shows that in terms of statistics, the measurement uncertainties are generally less than the dispersions of data of the three parameters. In this section, we are interested only in the general manner of the development of the three parameters. Therefore, considering the manner of development illustrated above (represented by the regression lines) is enough. Thus, let us consider a typical evolution of rest-frame indexes α_0 , β_0 , and peak energy $E_{0,p}$ following $\alpha_0 = -0.63 - 0.20(\tau_\theta - \tau_{\theta,1})/(\tau_{\theta,2} - \tau_{\theta,1})$, $\beta_0 = -2.44 - 0.42(\tau_\theta - \tau_{\theta,1})/(\tau_{\theta,2} - \tau_{\theta,1})$, and $\log(E_{0,p}/\text{keV}) = -0.06 - 0.16(\tau_\theta - \tau_{\theta,1})/(\tau_{\theta,2} - \tau_{\theta,1})$ for $\tau_{\theta,1} \leq \tau_\theta \leq \tau_{\theta,2}$ (to deduce the last formula, the previously adopted relation $E_p \simeq 1.67\Gamma E_{0,p}$ is applied to the typical hard burst, for which the Lorentz factor is assumed to be $\Gamma = 200$). For $\tau_\theta < \tau_{\theta,1}$, $\alpha_0 = -0.63$, $\beta_0 = -2.44$, and $\log(E_{0,p}/\text{keV}) = -0.06$, while for $\tau_\theta > \tau_{\theta,2}$, $\alpha_0 = -0.83$, $\beta_0 = -2.86$, and $\log(E_{0,p}/\text{keV}) = -0.22$. As mentioned above, we employ local Gaussian pulse of equation (3) with $\Delta\tau_{\theta, \text{FWHM}} = 0.1$ and assign $\tau_{\theta,0} = 10\sigma + \tau_{\theta, \text{min}}$ and $\tau_{\theta, \text{min}} = 0$ to study the relationship. We adopt $\tau_{\theta,1} = 9\sigma + \tau_{\theta, \text{min}}$ and $\tau_{\theta,2} = 11\sigma + \tau_{\theta, \text{min}}$. The corresponding relationships obtained in this situation are displayed in Figure 6. The deviation shown above is also observed in this figure. For the typical soft burst, the power-law range shifts to the *Swift* band as well. We find that the power-law index in the BATSE channels for the typical hard burst is within -0.27 to -0.08 .

We note that the peaked feature suggested above does not appear. Instead, both the lower and higher band plateaus shown

in Figures 4a and 4b remain. This might be due to the low speed of development of the rest-frame spectrum considered here (see below).

4. THE RELATIONSHIP SHOWN IN INDIVIDUAL PULSES OF A BATSE GRB SAMPLE

Presented in Kocevski et al. (2003) is a sample (the KRL sample) of FRED pulse GRBs. We consider only the first pulse of each burst since it is this pulse that is more closely associated with the initial condition of the event and might be less affected by environment. In addition, we limit our study to the sources for which the values of the peak energy are available and the corresponding signals are obvious enough so that the pulse widths of at least three BATSE channels can be well estimated. We find 28 bursts in the KRL sample that meet these requirements. For these sources, the peak energy values are taken from Mallozzi et al. (1995). To find the central values of data of the light curve, we simply adopt equation (22) of Kocevski et al. (2003) to fit the corresponding light curve since we find that the form of the function can well describe the observed profile of a FRED pulse. The pulse width in each BATSE channel is then estimated with the fitting parameters.

The estimated values of the FWHM of the 28 GRB pulses in various energy channels are presented in Table 3. The relationships between the pulse width and energy for these pulses are shown in Figure 7. Also plotted in Figure 7 are the limits of the corresponding power-law ranges of these pulses estimated with their peak energies according to the relations $\log E_{\text{low}} - \log E_p \simeq -1.10$ to -1.02 and $\log E_{\text{high}} - \log E_p \simeq 0.157$ to 0.177 , which are deduced from the typical rest-frame Band function spectrum

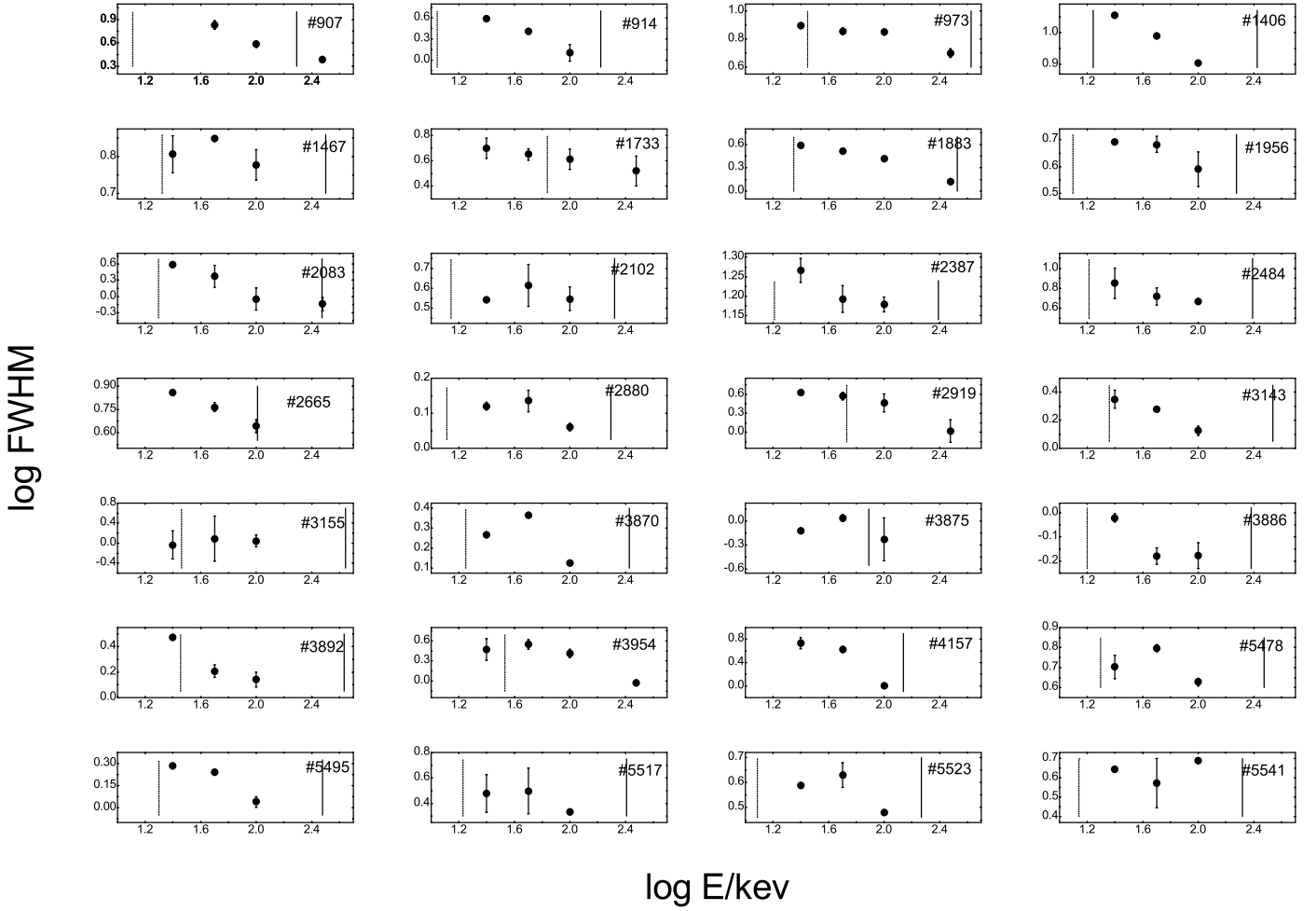


FIG. 7.—Relationship between the observed FWHM of pulses and energy shown in the BATSE energy range for the 28 GRBs concerned, where for some bursts the widths in all four BATSE channels are known while for others only the widths in three channels are available. The dashed vertical line represents the expected lower limit E_{low} of the power-law range, and the solid vertical line stands for the higher limit E_{high} ; the limits are associated with the typical rest-frame Band function spectrum with $\alpha_0 = -1$ and $\beta_0 = -2.25$ and the provided value of E_p .

with $\alpha_0 = -1$ and $\beta_0 = -2.25$ (see § 2.1), where only the largest value of E_{low} and the smallest value of E_{high} associated with the provided value of E_p are presented.

From Figure 7 we find the following:

1. A power-law range is observed in 13 sources: 907, 914, 1406, 1733, 1883, 2083, 2483, 2665, 2919, 3143, 3954, 4157, and 5495.
2. A lower band plateau is observed or suspected in eight bursts: 973, 1773, 1883, 1956, 2919, 3143, 4157, and 5495.
3. A higher band plateau is observed or suspected in six sources: 907, 2083, 2387, 2484, 3886, and 3892.
4. A peaked feature is observed or suspected in 10 GRBs: 1467, 2102, 2880, 3155, 3870, 3875, 3954, 5478, 5517, and 5523.

Among the 28 sources, those belonging to the plateau/power law/plateau feature group include 907, 914, 973, 1406, 1733, 1883, 1956, 2083, 2387, 2484, 2665, 2919, 3143, 3886, 3892, 4157, and 5495. Those belonging to the peaked feature class are 1467, 2102, 2880, 3155, 3870, 3875, 3954, 5478, 5517, and 5523. This suggests that the features shown in the relationship obtained from the 27 sources (called normal bursts) are those predicted by the Doppler effect of fireballs. The only exception is 5541, which shows a sinkage instead of a peaked feature in the relationship, which is not a result of our analysis.

In addition, we find that for 14 bursts (907, 914, 1406, 1733, 1883, 2083, 2387, 2484, 2665, 2919, 3143, 3892, 3954, and 5495), the power-law ranges expected from the range associated with the typical rest-frame Band function spectrum with $\alpha_0 = -1$ and $\beta_0 = -2.25$ and the provided value of E_p are consistent with what is derived from the observational data. For other normal bursts (there are 13), the two power-law ranges are not in agreement. Among these 13 normal bursts, the power-law range of burst 3886 is in a lower energy band than its E_p suggests, while for others, the power-law range is in a higher energy band than the provided value of E_p allows. If the relation (that is associated with the typical rest-frame Band function spectrum with $\alpha_0 = -1$ and $\beta_0 = -2.25$) used to derive the power-law range with the provided value of E_p is approximately applicable to these sources, the difference could be explained by assuming that the peak energies of these bursts have been underestimated. This assumption might be true since peak energies are always measured from time-integral spectra that must shift to a lower energy band from the hardest spectra of the sources. Under this interpretation, only the problem of the behavior of burst 3886 is unsolved.

5. DISCUSSION AND CONCLUSIONS

In this paper, we have studied in detail how the pulse width FWHM and the ratio of the rising width to the decaying width

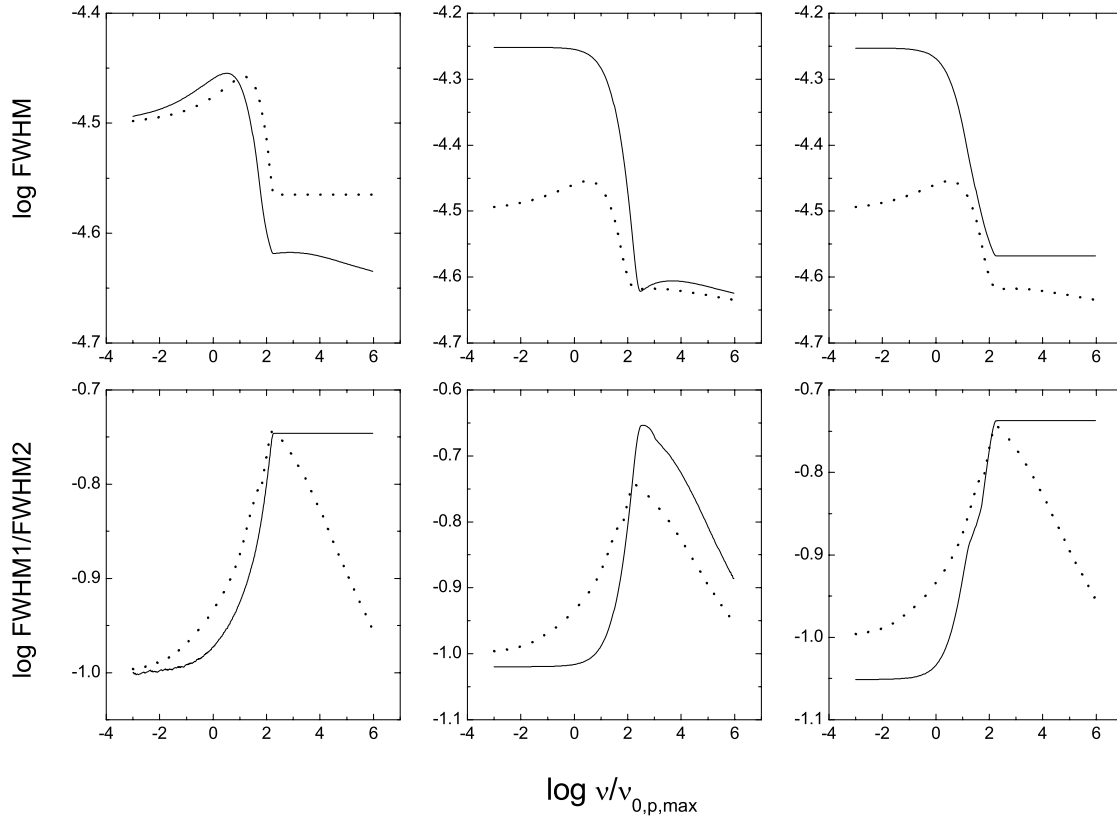


FIG. 8.—Relationships between the FWHM of pulses and energy (*top*) and between the ratio FWHM1/FWHM2 and energy (*bottom*) for the light curve of eq. (2) confined within $0.99\nu/\nu_{0,p} \leq \nu/\nu_{0,p} \leq 1.01\nu/\nu_{0,p}$, in the case of adopting various patterns of development of the Band function as the rest-frame radiation form and Gaussian pulse of eq. (3) with $\Delta\tau_{\theta,\text{FWHM}} = 0.1$ as its local pulse and taking $\Gamma = 100$ and $k = 1.0$. The solid lines in the left panels represent the curves associated with the case in which only the lower energy index varies with time; the solid lines in the middle panels represent those associated with the case in which only the higher energy index varies with time; the solid lines in the right panels stand for those associated with the case in which only the peak energy varies with time. The dotted lines represent the corresponding curves with $\Gamma = 100$ and $k = 1.0$ in Fig. 3 (i.e., the solid lines in the center panels of Fig. 3).

FWHM1/FWHM2 of GRBs are related to energy under the assumption that the sources are in the relativistically expanding fireball stage.

The following can be concluded from our analysis: (1) Owing to the Doppler effect of fireballs, it is common that there exists a power-law relationship between FWHM and energy and between FWHM1/FWHM2 and energy within a limited range of frequency. (2) The power-law range and index depend strongly on the rest-frame radiation form as well as the observed peak energy (the range spans more than 1–5 orders of magnitude in energy for different rest-frame spectra). (3) The upper and lower limits of the power-law range can be determined from the observed peak energy E_p . (4) In cases where the development of the rest-frame spectrum is ignored, a plateau/power law/plateau feature is formed, while in cases where the rest-frame spectrum is obviously softening with time, a peaked feature is observed. In addition, we find that local pulse forms affect only the magnitude of the width and the ratio of the widths.

We make predictions of the relationships for a typical hard burst with $\Gamma = 200$ and a typical soft burst with $\Gamma = 20$. The analysis shows that generally, for the typical hard burst the power-law range is observed in the BATSE band while for the typical soft burst the power-law range shifts to the *Swift* band. In some particular cases (e.g., when the rest-frame thermal synchrotron spectrum is adopted), the power-law range covers the BATSE as well as the *Swift* bands for both typical bursts.

A sample of 28 GRBs has been employed to study the relationship. We find that except for burst 5541, sources of the

sample either exhibit the plateau/power law/plateau feature (including 17 bursts) or show the peaked feature (including 10 bursts). This suggests that for most sources of this sample, the Doppler effect of fireballs could indeed account for the observed relationship. As for burst 5541, we wonder whether other kinds of rest-frame spectral evolution, such as a soft to soft manner instead of the simple decreasing pattern, could lead to its specific feature (this deserves further investigation). Since the peaked feature is a signature of the development of the rest-frame spectrum, we suspect that the 10 sources with the peaked feature might undergo an obvious evolution of radiation, while for the other 17 bursts, the development, if it exists, might be very mild.

In the above analysis, we consider the evolution of three parameters, the lower and higher energy indexes and the peak energy, of the rest-frame Band function spectrum. We wonder what role each of the three factors plays in producing the peaked feature shown above. Here we study once more the case of the simple evolution of indexes α_0 and β_0 and peak frequency $\nu_{0,p}$ considered in § 2.3, but in three different patterns. They are as follows: (1) $\alpha_0 = -0.5 - (\tau_\theta - \tau_{\theta,1})/(\tau_{\theta,2} - \tau_{\theta,1})$ for $\tau_{\theta,1} \leq \tau_\theta \leq \tau_{\theta,2}$, $\alpha_0 = -0.5$ for $\tau_\theta < \tau_{\theta,1}$, $\alpha_0 = -1.5$ for $\tau_\theta > \tau_{\theta,2}$, $\beta_0 = -2$, and $\log \nu_{0,p} = 0.1$; (2) $\beta_0 = -2 - (\tau_\theta - \tau_{\theta,1})/(\tau_{\theta,2} - \tau_{\theta,1})$ for $\tau_{\theta,1} \leq \tau_\theta \leq \tau_{\theta,2}$, $\beta_0 = -2$ for $\tau_\theta < \tau_{\theta,1}$, $\beta_0 = -3$ for $\tau_\theta > \tau_{\theta,2}$, $\alpha_0 = -0.5$, and $\log \nu_{0,p} = 0.1$; (3) $\log \nu_{0,p} = 0.1 - (\tau_\theta - \tau_{\theta,1})/(\tau_{\theta,2} - \tau_{\theta,1})$ for $\tau_{\theta,1} \leq \tau_\theta \leq \tau_{\theta,2}$, $\log \nu_{0,p} = 0.1$ for $\tau_\theta < \tau_{\theta,1}$, $\log \nu_{0,p} = 1.1$ for $\tau_\theta > \tau_{\theta,2}$, $\alpha_0 = -0.5$, and $\beta_0 = -2$. The first pattern is associated with the evolution of the lower energy index of the rest-frame Band function spectrum,

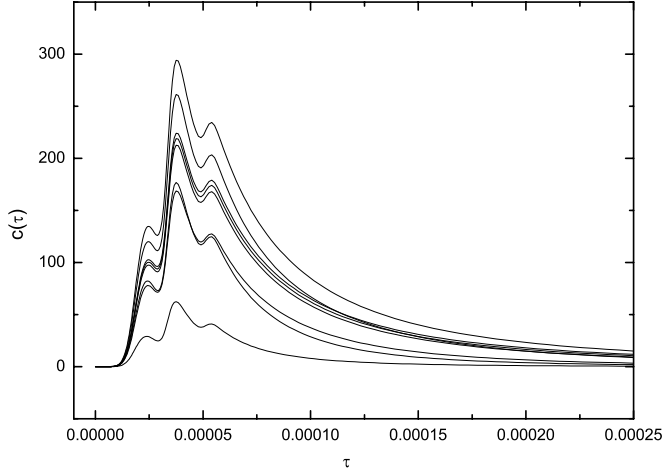


FIG. 9.—Light curves in channels B, E, A, C, D, F, G, and H (*top to bottom*) for the typical hard burst ($\Gamma = 200$). The curves are calculated with eq. (2) when adopting the local pulse comprising the three Gaussian forms shown by eq. (7) and the rest-frame Band function with $\alpha_0 = -1$, $\beta_0 = -2.25$, and $\nu_{0,p} = 0.75 \text{ keV h}^{-1}$.

the second reflects nothing but the evolution of the higher energy index of the same, and the third connects with the evolution of the peak energy of the same, where for each of the three cases, the other two parameters are fixed. In the same way we employ the local Gaussian pulse of equation (3) with $\Delta\tau_{\theta,\text{FWHM}} = 0.1$ to study the relationship. We adopt $\Gamma = 100$, $\tau_{\theta,1} = 9\sigma + \tau_{\theta,\min}$, and $\tau_{\theta,2} = 11\sigma + \tau_{\theta,\min}$, and assign $\tau_{\theta,0} = 10\sigma + \tau_{\theta,\min}$ and $\tau_{\theta,\min} = 0$. Displayed in Figure 8 are the corresponding $\text{FWHM1}/\nu_{0,p,\max}$ and $\text{FWHM1}/\text{FWHM2}-\nu_{0,p,\max}$ curves, where $\nu_{0,p,\max}$ is the largest value of $\nu_{0,p}$ adopted. One finds from Figure 8 that the peaked feature shown in the relationship between the width and energy (see Fig. 3) is mainly due to the evolution of the lower energy index of the rest-frame Band function spectrum, while that shown in the relationship between the ratio of pulse widths and energy arises from the evolution of the higher energy index. It is interesting that no contribution from the evolution of the peak energy of the rest-frame Band function spectrum to the features is detected (probably the evolution of the peak energy considered here is too mild to produce an interesting feature).

As mentioned above, it has been proposed by many authors that the power-law relationship observed in GRB pulses could arise from synchrotron radiation (see § 1). A simple synchrotron cooling scenario is that as the electrons cool, their average energy becomes smaller, which causes the emission peaks at lower energy at later times (see Kazanas et al. 1998). Recently, a power-law relationship between the total isotropic energy and E_p was revealed (Lloyd et al. 2000; Amati et al. 2002). It has been suggested that this power-law relation can be expected in the case of an optically thin synchrotron shock model for a power-law distribution of electrons (see Lloyd et al. 2000). These considerations lead to a softening picture of the rest-frame spectrum.

Does the proposal of synchrotron radiation conflict with the effect discussed above? To find an answer to this, it might be helpful to recall that the Doppler effect of fireballs is only a kinetic effect while that of synchrotron radiation is a dynamic one. Therefore, there is no conflict between the two. As analyzed in § 2.3, a softening of the rest-frame spectrum coupled with the Doppler effect of fireballs would lead to a peaked feature in the relationship between the pulse width and energy if the speed of the softening is fast enough. The observed data of our sample (see Fig. 7) show that this is indeed the case for some events (at least for some FRED pulse GRBs).

We wonder whether the softening of the rest-frame spectrum could lead to a much different value of the power-law index. We thus analyze the power-law ranges in the top panels of Figure 3 and find that the index is confined within -0.27 to -0.18 , which is not very different from what was obtained above.

We know that light curves of most bursts are complex and do not consist of single pulses. It has been pointed out that the superposition of many pulses could create the observed diversity and complexity of GRB light curves (Fishman et al. 1994; Norris et al. 1996; Lee et al. 2000a, 2000b). Could our analysis be applied to all light curves observed in GRBs? The answer is no. The Doppler effect of fireballs is associated with the angular spreading timescale, which is proportional to $1/2\Gamma^2$ (see, e.g., Kobayashi et al. 1997; Piran 1999; Nakar & Piran 2002; Ryde & Petrosian 2002). Our model would not be applicable to light curves of multipulses, which are separated by timescales larger than the angular spreading timescale.

What would happen if local pulses are close enough? Let us consider a local pulse comprising three Gaussian forms:

$$\begin{aligned} \tilde{I}(\tau_\theta) = & I_{0,1} \exp \left[- \left(\frac{\tau_\theta - \tau_{\theta,0,1}}{\sigma_1} \right)^2 \right] \\ & + I_{0,2} \exp \left[- \left(\frac{\tau_\theta - \tau_{\theta,0,2}}{\sigma_2} \right)^2 \right] + I_{0,3} \exp \left[- \left(\frac{\tau_\theta - \tau_{\theta,0,3}}{\sigma_3} \right)^2 \right], \\ & \tau_{\theta,\min} \leq \tau_\theta, \end{aligned} \quad (7)$$

where $I_{0,1}$, $I_{0,2}$, $I_{0,3}$, σ_1 , σ_2 , σ_3 , $\tau_{\theta,0,1}$, $\tau_{\theta,0,2}$, $\tau_{\theta,0,3}$, and $\tau_{\theta,\min}$ are constants. We calculate the light curves of equation (2) arising from the local pulse of equation (7) and emitted with the typical rest-frame Band function spectral form with $\alpha_0 = -1$ and $\beta_0 = -2.25$, adopting $I_{0,1} = 0.15$, $I_{0,2} = 0.2$, $I_{0,3} = 0.04$, $\sigma_1 = 0.3$, $\sigma_2 = 0.2$, $\sigma_3 = 0.2$, $\tau_{\theta,0,1} = 5\sigma_1 + \tau_{\theta,\min}$, $\tau_{\theta,0,2} = \tau_{\theta,0,1} + 4\sigma_1$, $\tau_{\theta,0,3} = \tau_{\theta,0,2} + 7\sigma_2$, $\nu_{0,p} = 0.75 \text{ keV h}^{-1}$, and $\Gamma = 200$, and assigning $\tau_{\theta,\min} = 0$. In Figure 9 we show the corresponding light curves in channels A, B, C, D, E, F, G, and H, and in Figure 10 we present the relationships between $\text{FWHM}/\text{FWHM}_E$ and E/keV and between $\text{FWHM1}/\text{FWHM2}$ and E/keV deduced from these light curves. We find no significant difference between

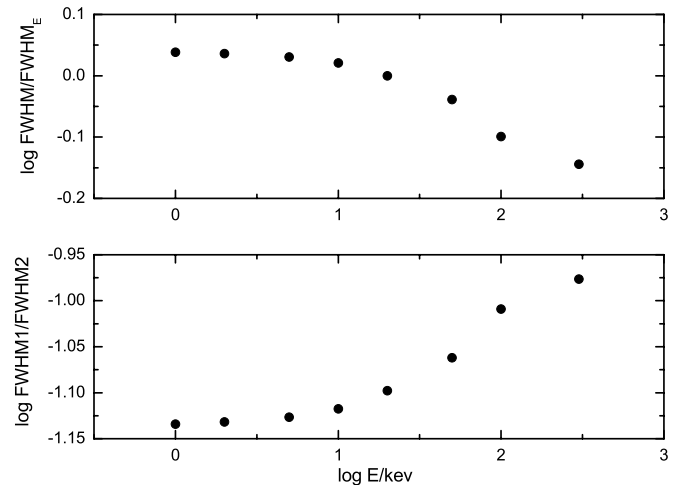


FIG. 10.—Prediction of the relationships between the width of pulses and energy (*top*) and between the ratio of the FWHM of the rising portion to that of the decaying phase of the light curve of pulses, on one hand, and energy, on the other (*bottom*), for the typical hard burst. The widths are deduced from the light curves of Fig. 9.

these relationships and those in Figure 4 (the data of the typical hard burst there).

It should be pointed out that in this paper we are interested in cases where the Doppler effect of fireballs is important and thus we examine only FRED pulse sources. It would not be surprising if the results are not applicable to other forms of pulses. In the case where the mentioned effect is not at work, a power-law relationship might also exist. If so, synchrotron radiation might be responsible for the observed relationship. This, we believe, also

deserves a detailed investigation (probably, in this case, the pulses concerned should be non-FRED ones).

Our thanks are given to B. Paciesas for providing us the necessary peak energy data. This work was supported by the Special Funds for Major State Basic Research Projects (“973”) and the National Natural Science Foundation of China (grant 10273019).

REFERENCES

- Amati, L., et al. 2002, *A&A*, 390, 81
 Band, D., et al. 1993, *ApJ*, 413, 281
 Chiang, J. 1998, *ApJ*, 508, 752
 Cohen, E., Katz, J. I., Piran, T., & Sari, R. 1997, *ApJ*, 488, 330
 Costa, E. 1998, *Nucl. Phys. B (Proc. Suppl.)*, 69(1–3), 646
 Crew, G. B., et al. 2003, *ApJ*, 599, 387
 Dado, S., Dar, A., & De Rujula, A. 2002a, *A&A*, 388, 1079
 ———. 2002b, *ApJ*, 572, L143
 Dermer, C. D. 1998, *ApJ*, 501, L157
 Eriksen, E., & Gron, O. 2000, *Am. J. Phys.*, 68, 1123
 Fenimore, E. E., in ‘t Zand, J. J. M., Norris, J. P., Bonnell, J. T., & Nemiroff, R. J. 1995, *ApJ*, 448, L101
 Fenimore, E. E., Madras, C. D., & Nayakshin, S. 1996, *ApJ*, 473, 998
 Feroci, M., et al. 2001, *A&A*, 378, 441
 Fishman, G. J., Meegan, C. A., Wilson, R. B., Horack, J. M., Brock, M. N., Paciesas, W. S., Pendleton, G. N., & Kouveliotou, C. 1992, in *AIP Conf. Proc.* 258, *Gamma-Ray Bursts*, ed. W. S. Paciesas & G. J. Fishman (New York: AIP), 13
 Fishman, G. J., et al. 1994, *ApJS*, 92, 229
 Goodman, J. 1986, *ApJ*, 308, L47
 Granot, J., Piran, T., & Sari, R. 1999, *ApJ*, 513, 679
 Hailey, C. J., Harrison, F. A., & Mori, K. 1999, *ApJ*, 520, L25
 Kazanas, D., Titarchuk, L. G., & Hua, X.-M. 1998, *ApJ*, 493, 708
 Kobayashi, S., Piran, T., & Sari, R. 1997, *ApJ*, 490, 92
 Kocevski, D., Ryde, F., & Liang, E. 2003, *ApJ*, 596, 389
 Krolik, J. H., & Pier, E. A. 1991, *ApJ*, 373, 277
 Lee, A., Bloom, E. D., & Petrosian, V. 2000a, *ApJS*, 131, 1
 ———. 2000b, *ApJS*, 131, 21
 Liang, E. P., Jernigan, T. E., & Rodrigues, R. 1983, *ApJ*, 271, 766
 Link, B., Epstein, R. I., & Priedhorsky, W. C. 1993, *ApJ*, 408, L81
 Lloyd, N. M., Petrosian, V., & Mallozzi, R. S. 2000, *ApJ*, 534, 227
 Mallozzi, R. S., Paciesas, W. S., Pendleton, G. N., Briggs, M. S., Preece, R. D., Meegan, C. A., & Fishman, G. J. 1995, *ApJ*, 454, 597
 Mészáros, P., & Rees, M. J. 1998, *ApJ*, 502, L105
 Nakar, E., & Piran, T. 2002, *ApJ*, 572, L139
 Nemiroff, R. J. 2000, *ApJ*, 544, 805
 Norris, J. P., Marani, G. F., & Bonnell, J. T. 2000, *ApJ*, 534, 248
 Norris, J. P., Nemiroff, R. J., Bonnell, J. T., Scargle, J. D., Kouveliotou, C., Paciesas, W. S., Meegan, C. A., & Fishman, G. J. 1996, *ApJ*, 459, 393
 Paczyński, B. 1986, *ApJ*, 308, L43
 Piran, T. 1999, *Phys. Rep.*, 314, 575
 Piro, L., et al. 1998, *A&A*, 329, 906
 Preece, R. D., Briggs, M. S., Mallozzi, R. S., Pendleton, G. N., Paciesas, W. S., & Band, D. L. 2000, *ApJS*, 126, 19
 Qin, Y.-P. 2002, *A&A*, 396, 705
 ———. 2003, *A&A*, 407, 393
 Qin, Y.-P., Zhang, Z.-B., Zhang, F.-W., & Cui, X.-H. 2004, *ApJ*, 617, 439 (Paper I)
 Ryde, F., & Petrosian, V. 2002, *ApJ*, 578, 290
 Schaefer, B. E., et al. 1994, *ApJS*, 92, 285
 Shen, R.-F., Song, L.-M., & Li, Z. 2005, *MNRAS*, 362, 59
 Strohmayer, T. E., Fenimore, E. E., Murakami, T., & Yoshida, A. 1998, *ApJ*, 500, 873
 Wang, J. C., Cen, X. F., Qian, T. L., Xu, J., & Wang, C. Y. 2000, *ApJ*, 532, 267